# Nanoscale

Accepted Manuscript


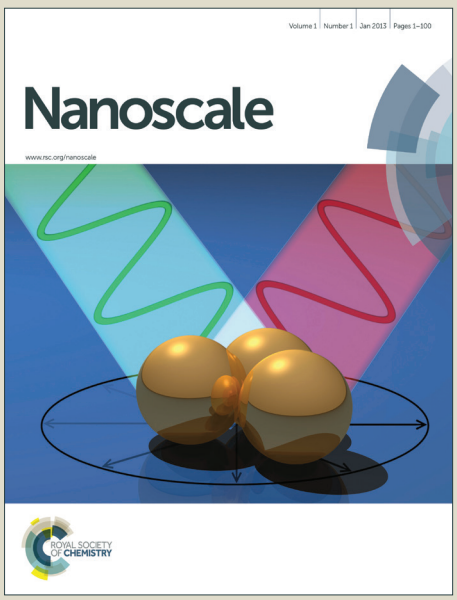





ROYAL SOCIETY OF CHEMISTRY

www.rsc.org/nanoscale

Cite this: DOI: 10.1039/c0xx00000x

www.rsc.org/xxxxxx

PAPER

# Optimized performances of tetrapod-like ZnO nanostructure for triode structure field emission planar light source

**Yiren Chen,[a] Liqin Hu,[b] Hang Song,*[a] Hong Jiang,[a] Dabing Li,*[a] Guoqing Miao,[a] Zhiming Li,[a] Xiaojuan Sun,[a] Zhiwei Zhang[a] and Tailiang Guo*[b]**

***Received (in XXX, XXX) Xth XXXXXXXXX 20XX, Accepted Xth XXXXXXXXX 20XX***
**DOI: 10.1039/b000000x**

Tetrapod-like ZnO (T-ZnO) nanostructures were synthesized by simple vapor phase oxidation method without any catalysts or additives. We optimized the performances of T-ZnO nanostructures through adjusting the partial pressure of Zn vapour in the total pressure of quartz chamber and obtained high purity, uniform morphology and size and high aspect ratio T-ZnO nanostructure materials with low turn-on electric field of 2.75 V $\mu m^{-1}$, large field enhancement factor of 3410 and good field emission stability for more than 70 hours continuous emission. Besides, based on the optimized T-ZnO, we developed metal grid mask-assisted water-based electrostatic spraying technology, and fabricated large-scale, pollution-free, hole-shaped arrays T-ZnO nanostructure cathode used in a triode structure field emission planar light source. The controllable performances of triode device were intensively investigated and the results showed that the triode device uniformly illuminated with luminous intensity as high as 8000 cd $m^{-2}$ under the conditions of 200 V grid voltage and 3300 V anode voltage. The research in this paper will benefit the development of high performance planar light source based on T-ZnO nanostructures.

## Introduction

Due to the chemical stability, wide direct band gap, large exciton binding energy, high aspect ratio and controllable size, zinc oxide (ZnO) nanostructures have been considered to be one of the most promising materials for nanoscale electronic and optoelectronic devices.[1] Among various morphologies of ZnO, tetrapod-like ZnO (T-ZnO) nanostructure has attracted considerable attention. So far, T-ZnO nanostructure has been extensively investigated in gas sensors,[2,3] ultraviolet (UV) photodetectors,[4-6] field effect transistors,[7] nanoscale logic devices[8] and dye-sensitized solar cells.[9] The intrinsic three-dimensional (3D) spacial structure of T-ZnO with four needle-shaped legs distributing in tetrahedral angles and nanoscale tips is beneficial for the application as cold cathode material in field-emission-based devices such as field emission display (FED), cathodoluminescence, field emission planar light source, electron microscope, etc.[10] As a matter of fact, many studies on T-ZnO nanostructures as field emitters have been carried out.[11-13] However, the features of T-ZnO nanostructures such as morphology, size, purity and aspect ratio presented great difference and the field emission often exhibited poor stability due to the effect of adsorbates on T-ZnO nanostructures introduced in the process of transfer.[14] Moreover, the reported structure of field emission device based on T-ZnO nanostructure was mainly limited to the simple diode structure which suffered from poor emission uniformity and low luminous efficiency.

In this letter, we firstly grew T-ZnO nanostructures by simple controllable vapour phase oxidation method without any catalysts or additives and obtained high purity, uniform morphology and size, high aspect ratio and good field emission characteristics T-ZnO nanostructure materials by adjusting the partial pressure of Zn vapour in the total pressure of quartz chamber. Then, the optimized T-ZnO nanostructure materials were transferred to hole-shaped Ag cathode by metal grid mask-assisted water-based electrostatic spraying method which was superior to the methods of screen-printing T-ZnO and organic solvent hybrid reported by Lei et al.[15] and metal-cation-assisted electrophoretic deposition.[16,17] The screen-printing and electrophoretic deposition methods introduced additives so that affected the emission stability. Finally, a field emission planar light source based on metal grid triode structure was fabricated, which overcame the disadvantages of simple diode structure and realized practicable, efficient, and uniform lighting. Through the *in-situ* comparatively studying the performance of the triode structure light source, we demonstrated that the optimum performance could be obtained by controlling the grid voltage working at the saturation region.

## Experimental section

### Preparation of T-ZnO nanostructure materials

T-ZnO nanostructures were synthesized by simple controllable vapour phase oxidation method using low vacuum horizontal tube furnace. In the process of material preparation, the ceramic plate held with high purity zinc powder (purity: 99.99%) was pre-placed into quartz tube and the flow rates of Ar and $O_2$ were adjusted to 200 sccm and 10 sccm, respectively. Before heating up, the chamber was pumped to the pressure of 500, 200, 100 and

20 Pa, respectively. Then, the temperature was increased at a rate of 100 °C min$^{-1}$ and kept at 950 °C for 60 min. By changing the chamber pressure so as to adjust the partial pressure of Zn vapour, we obtained different T-ZnO nanostructures with chamber pressure at 500, 200, 100 and 20 Pa, corresponding to sample A, B, C and D, respectively. The effect of the chamber pressure on the morphology of T-ZnO nanostructures could be investigated.

**Fabrication of triode structure field emission device**

The Ag strip electrodes were used as cathodic electrodes of triode structure. At first, we obtained periodic hole-shaped array cathodic electrodes by fabricating hole-shaped insulator layer on Ag electrodes in terms of thick film screen-printing process and high temperature sintering. Then, T-ZnO nanostructures were dispersed in deionized water by ultrasonic and formed T-ZnO suspension of 0.05 wt%. Using the method of electrostatic spraying, the T-ZnO suspension was transferred to hole-shaped Ag electrodes and dried at 100 °C for 30 min. In the spraying process, hole-shaped metal grid was used as a mask to ensure that T-ZnO nanostructures were only sprayed in the holes. After finishing the preparation of T-ZnO field emission cathode, it was combined with hole-shaped metal grid and fluorescent screen to assemble triode structure device. The metal grid was directly placed on the insulator layer while the fluorescent screen kept a space of 500 μm from metal grid.

**Characterization and measurement**

The morphology and structure of T-ZnO nanostructures were characterized by scanning electron microscopy (SEM, Hitachi S-4800) and X-ray diffraction (XRD, Bruker D8). The field emission property of sample A, B, C and D was investigated by current density-electric field (*J-E*) characteristic which was carried out in the diode structure and measured under the conditions of 9 x 10$^{-5}$ Pa vacuum pressure, 3 mm x 3 mm effective field emission area and 200 μm distance between cathode and anode. The field enhancement factors ($\beta$) of four samples were calculated by Fowler-Nordheim (FN) equation. All of the electrical properties, including *J-E* and electron emission stability (*J-T*) were characterized by Agilent testing system. In addition, the parameters and morphology of hole-shaped dielectric layer in triode structure were characterized by step profiler (Vecco Dekatk150).

## Results and discussion

Fig. 1 shows a typical XRD pattern of the synthesized T-ZnO nanostructure and its macro morphology which looks like white cotton. The positions of the XRD peaks corresponding to (100), (002), (101), (102), (110) and (103) planes are well consistent with those of the hexagonal wurtzite-structured ZnO (Joint Committee for Powder Diffraction Standards (JCPDS): Card No. 36-1451). Its lattice constants are calculated to be 0.3248 and 0.5205 nm for a- and c-axis, respectively, using the Bragg diffraction equation and lattice constant formula of hexagonal system[18,19] described as follows:

$$2d_{(hkl)} \cdot \sin\theta_{(hkl)} = \lambda \quad (1)$$

and

$$\frac{1}{d^2_{(hkl)}} = \frac{4 \cdot (h^2 + k^2 + hk)}{3a^2} + \frac{l^2}{c^2} \quad (2)$$

Where *(hkl)* is on behalf of Miller indices, $d_{(hkl)}$ is the interplanar spacing, $\theta_{(hkl)}$ is the angle between the incident X-ray and *(hkl)* crystal face and $\lambda$ (= 0.15406 nm) is the wavelength of X-ray.

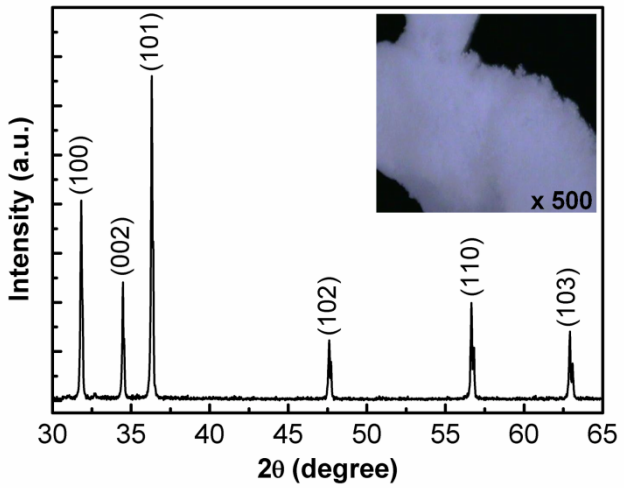


**Fig. 1** The typical XRD pattern of the as-grown T-ZnO nanostructure. The inset shows its macro morphology under 500 times microscopy which looks like cotton.

The T-ZnO nanostructures with different morphologies are synthesized by adjusting the chamber pressure at 500, 200, 100 and 20 Pa, as shown in Fig. 2(a)-(d). The morphologies of T-ZnO nanostructures change along with the variation of chamber pressure which mainly lies in the adjustment of the Zn partial pressure.[10,20-22] As per the laws of vacuum,[23] in a certain temperature, lower the chamber pressure, higher is the evaporation rate of Zn, thus resulting into higher partial pressure of Zn vapour. On the contrary, higher chamber pressure results in lower partial pressure of Zn vapour. Under high chamber pressure, compared with the low Zn partial pressure, the supply of $O_2$ is adequate, therefore, the needles of T-ZnO grow enough or even excessively that appear butterfly-shaped T-ZnO nanostructure, as shown in Fig. 2(a). With the chamber pressure decreasing, the Zn partial pressure increases. In this process, the supply of $O_2$ undergoes the transition from sufficiency to moderation firstly which results in good orientated growth of whisker and obtains T-ZnO nanostructures with uniform morphology and high purity, as shown in Fig. 2(b) and (c). When the chamber pressure further decreasing, the partial pressure of $O_2$ is relatively insufficient and cannot meet the need of the whisker growth, the result leads to the bad orientated growth of whisker and generate ZnO particles in the product, as shown in Fig. 2(d). In other words, the T-ZnO nanostructures with uniform morphology can be fabricated at proper Zn partial pressure by well controlling the chamber pressure. In addition, as the partial pressure of Zn vapour increases, the lateral growth of needles of T-ZnO nanostructure gradually becomes remarkable so that the needles grow thickly. The lateral growth will affect the curvature radius of needles of T-ZnO nanostructure so as to its field enhancement factor.

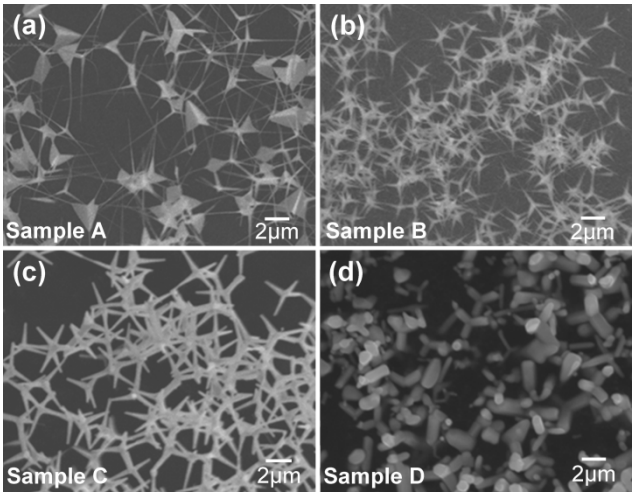


**Fig. 2** SEM images of T-ZnO nanostructures under different chamber pressures: (a) 500 Pa, (b) 200 Pa, (c) 100 Pa, and (d) 20 Pa, respectively.

The field emission properties of Sample A, B, C and D are demonstrated in Fig. 3(a) and (b). As shown in Fig. 3(a), different *J-E* curves are presented. The turn-on electric field ($E_{TO}$) is conventionally defined as the electric field at the field emission current density of 10 μA $cm^{-2}$.[24] Therefore, we get the $E_{TO}$ of four samples at 3.5 V $\mu m^{-1}$, 2.75 V $\mu m^{-1}$, 3.9 V $\mu m^{-1}$ and 7.4 V $\mu m^{-1}$, corresponding to sample A, B, C and D, respectively. Moreover, the field emission characteristics can be evaluated by the FN model. According to typical FN theory, the field emission current density *J* can be described as the equation of electric field *E*:[10,25-27]

$$J = \frac{A\beta^2 E^2}{\emptyset} \cdot exp\left(\frac{-B\emptyset^{3/2}}{\beta E}\right) \quad (3)$$

or

$$ln\frac{J}{E^2} = ln\frac{A\beta^2}{\emptyset} - \frac{B\emptyset^{3/2}}{\beta E} \quad (4)$$

where *A* and *B* are constants with the value of $1.56 \times 10^{-10}$ A $V^{-2}$ eV and $6.83 \times 10^3$ V $eV^{-3/2}$ $\mu m^{-1}$, respectively. $\Phi$ is the work function of the material which is 5.3 eV for ZnO.[28] $\beta$ is the field enhancement factor related to the aspect ratio and curvature radius of needles of T-ZnO nanostructures. By plotting $\ln(J/E^2)$ *versus 1/E*, we obtain FN plots of four samples, as shown in Fig. 3(b). The observed FN plots exhibit deviation from linearity at high field region which can be ascribed to the semiconducting nature of T-ZnO involved in the characteristic of the energy band structure and voltage-to-barrier-field conversion factor.[13,27] From the slope of FN plots, the field enhancement factors of four samples (designated as $\beta_A$, $\beta_B$, $\beta_C$ and $\beta_D$) are estimated to be 2812, 3410, 2431 and 905, respectively. Sample B presents a higher field enhancement factor due to the advantage of its geometry fabricated at proper Zn partial pressure. Besides, the field emission stability of sample B is also confirmed by *J-T* measurement, as illustrated in Fig. 3(c). The measurement is carried out at 1100 V for more than 70 h. Its current density undergoes a slight decrease at first, and then turns to stabilization as time going on. In a word, sample B exhibits excellent characteristics such as uniform morphology and size, low turn-on electric field, large field enhancement factor and good stability which are better than the reported properties of other-shaped ZnO nanostructures[10,29,30] and beneficial to use as field emitter.

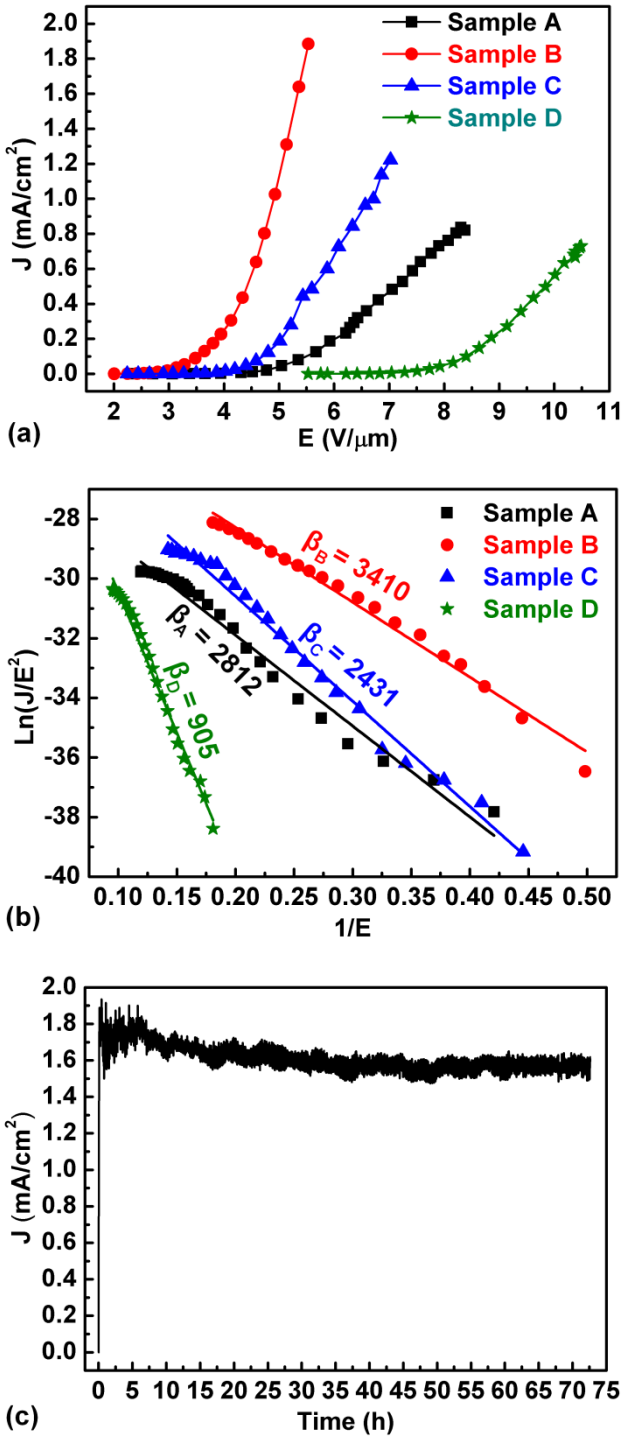


**Fig. 3** Field emission properties of Sample A, B, C and D: (a) the *J-E* curves, (b) corresponding FN plots and (c) the *J-T* curve of Sample B.

We fabricate a field emission planar light source based on metal grid triode structure using the T-ZnO nanostructure of sample B as the field emitter. The structural schematic diagram of triode device is shown in Fig. 4(a). The preparation of physical device has been introduced in the experimental section above in

detail. Herein, as illustrated in Fig. 4(b), the 500 times microscopy image of hole-shaped insulator layer is presented. The dimension of insulator hole is 600 μm for bottom diameter with a period of 1 mm and the layer thickness is about 12 μm, as measured by step profiler in Fig. 4(d). Fig. 4(c) exhibits the SEM image of hole-shaped Ag electrode in local area. As can be seen, T-ZnO nanostructures with 2-μm-long needles are distributed on the surface of Ag electrode uniformly and uprightly. In addition, the used metal grid has hole-shaped arrays with 600-μm-diameter, 1-mm-period and 100-μm-thickness, as shown in Fig. 4(e).

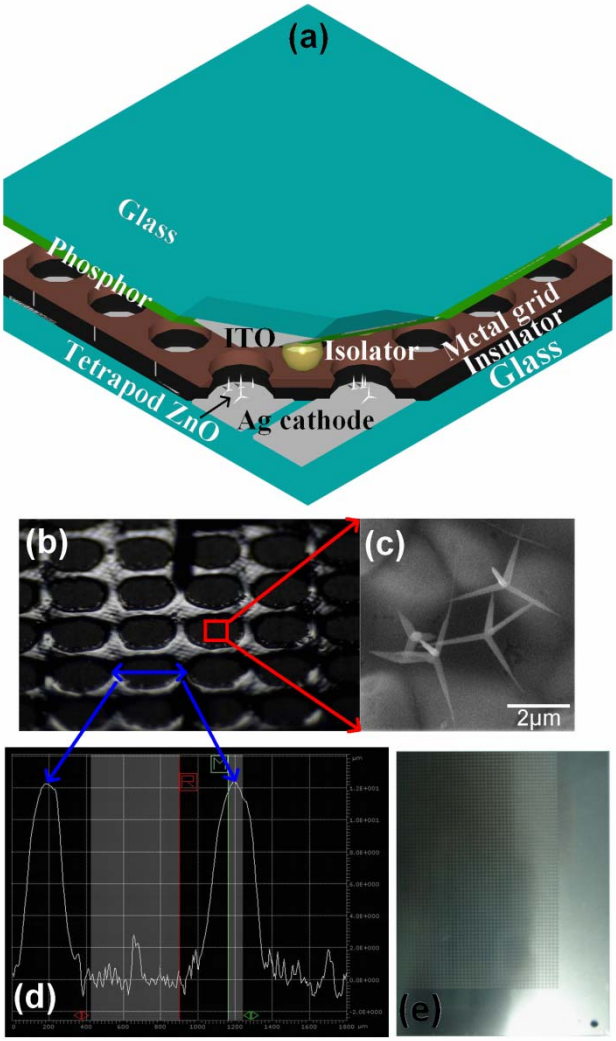


**Fig. 4** (a) The structural schematic diagram of triode device; (b) image of hole-shaped insulator layer under 500 times microscopy; (c) the SEM image of T-ZnO nanostructures located at the surface of hole-shaped Ag electrode; (d) the dimension of insulator hole; (e) hole-shaped metal grid used in triode structure.

The performance of triode structure device is investigated by current-voltage (*I-V*) under the condition of 9 x $10^{-5}$ Pa vacuum pressure. The electrical connection in triode structure is shown in the inset of Fig. 5. Fixing the voltage of anode fluorescent screen ($V_A$) at 3300 V, we obtain the relationships of anode current ($I_A$) *versus* grid voltage ($V_G$), cathode current ($I_C$) *versus* $V_G$ and grid current ($I_G$) *versus* $V_G$ by adjusting the $V_G$ from 0 V to 200 V, as shown in Fig. 5. With the increase of $V_G$, the $I_C$ increases while the $I_A$ undergoes the process of increasing at first, and then tending to saturation. We define four points labelled as a, b, c and d (pointed by green arrows) on $I_A$ *versus* $V_G$ curve, corresponding to $V_G$ = 0 V, 100 V, 150 V and 200 V, respectively, and record their field emission images in Fig. 6(a)-(d) for *in-situ* comparative study. As can be seen from Fig. 6(a), $V_G$ = 0 V which means that the triode device behaves as the diode structure, the uniformity of luminance is poor. When applying 100 V to $V_G$, the modulating electric field formed by $V_G$ (about 8.33 V $\mu m^{-1}$) slightly improves the uniformity of luminance, as shown in Fig. 6(b). In Fig. 6(c), when $V_G$ is further increased to 150 V, the modulation effect of $V_G$ is obvious that the device emerges large-scale uniform luminance with brightness of 7200 cd $m^{-2}$. At this point, $I_A$ and $I_C$ increase dramatically. With the further increase of $V_G$ to 200 V, corresponding to the modulating electric field of 16.67 V $\mu m^{-1}$, though the luminous intensity still has a certain level enhancement with brightness reaching up to 8000 cd $m^{-2}$ in Fig. 6(d), comparing with Fig. 6(c), $I_A$ tends to saturation. However, $I_C$ keeps on increasing in this process. That is to say, the modulation effect of grid voltage to anode current has a limit under a specific anode voltage.

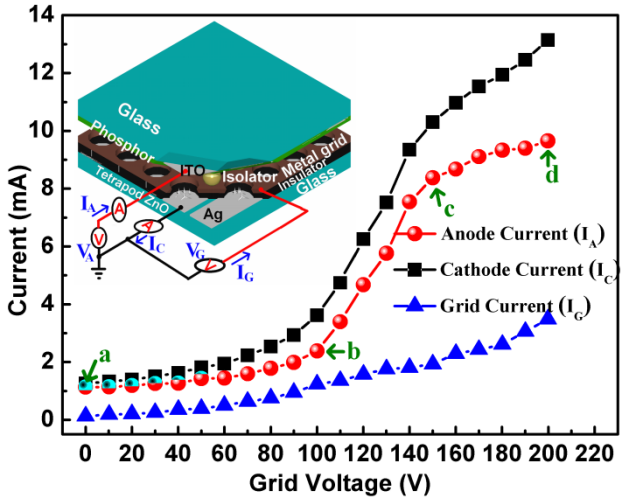


**Fig. 5** The relationships of anode current ($I_A$) *versus* grid voltage ($V_G$), cathode current ($I_C$) *versus* $V_G$ and grid current ($I_G$) *versus* $V_G$ when fixing anode voltage ($V_A$) at 3300 V. The inset is the electrical connection in triode structure.

The main reason for the saturation of $I_A$ lies in that: with the increase of $V_G$, the electric field at the tips of T-ZnO nanostructures is enhanced gradually so that more and more electrons will obtain sufficient energy to overcome the barrier of T-ZnO and emit into vacuum to form free electrons. These free electrons move directionally under the accelerating field formed by $V_A$ and generate cathode current $I_C$. The $I_C$ can be described as $I_C = I_A + I_G$. When $V_G$ is relatively small, the ability of metal grid to attract electrons is weak, so the difference between $I_A$ and $I_C$ is not obvious. With the further increase of $V_G$, when it reaches a certain value (such as 150 V in this paper), although the $I_C$ largely increases, the ability of metal grid to attract electrons is also enhanced, which weakens the focussing of electron trajectories and captures more and more electrons. Therefore, the $I_G$ substantially increases to restrain the increase of $I_A$. It results in the saturation of $I_A$. On the other hand, the weak focussing of electron trajectories leads to relative large electron beam spots

which stimulate the anode fluorescent screen and improve the uniformity of luminance.

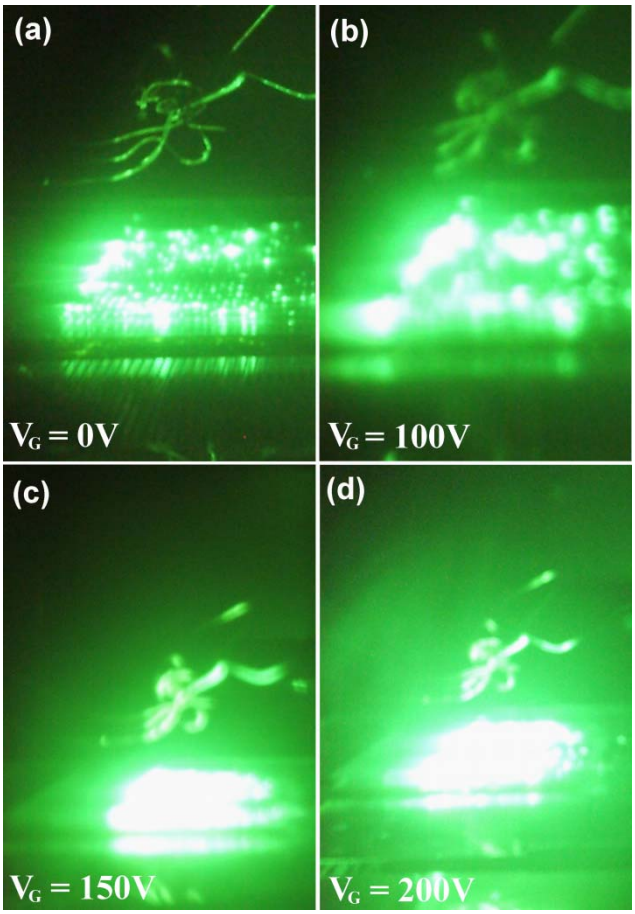


**Fig. 6** The field emission images at $V_A$ = 3300 V and (a) $V_G$ = 0 V, (b) $V_G$ = 100 V, (c) $V_G$ = 150 V and (d) $V_G$ = 200 V.

## Conclusions

Through adjusting the partial pressure of Zn vapour in the total pressure of quartz chamber, the excellent characteristics of T-ZnO nanostructure materials were synthesized by simple vapor phase oxidation method without any catalysts or additives. The optimized T-ZnO nanostructures presented low turn-on electric field of 2.75 V $\mu m^{-1}$, large field enhancement factor of 3410 and excellent field emission stability for more than 70 h continuous emission, in addition to the uniform morphology and size. Based on the optimized T-ZnO, we developed metal grid mask-assisted water-based electrostatic spraying technology, and fabricated large-scale, pollution-free, hole-shaped arrays T-ZnO nanostructure cathode. A triode structure field emission planar light source was assembled using T-ZnO nanostructure cathode, hole-shaped metal grid and fluorescent screen. Through the *in-situ* comparatively studying the performance of the triode structure light source, we demonstrated that the optimum performance could be obtained by controlling the grid voltage working at the saturation region. As the experimental results shown, the triode structure light source uniformly illuminated with luminous intensity as high as 8000 cd $m^{-2}$ under the conditions of 200 V grid voltage and 3300 V anode voltage. It is believed that the research in this paper will benefit the development of novel, high performance planar light source based on T-ZnO nanostructures.

## Acknowledgements

This work is supported by the National Basic Research Program of China (973 Program, Grant No. 2010CB327705) and the Jilin Provincial Science & Technology Department (Grant No. 20140520116JH).

## Notes and references

[a] *State Key Laboratory of Luminescence and Applications, Changchun Institute of Optics, Mechanics and Physics, Chinese Academy of Sciences, 3888 Dongnanhu Road, Changchun 130033, People's Republic of China. E-mail: songh@ciomp.ac.cn, lidb@ciomp.ac.cn and gtl@fzu.edu.cn*
[b] *College of Physics and Information Engineering, Fuzhou University, 523 Industrial Road, Fuzhou 350002, People's Republic of China*

1 N. Pan, X. P. Wang, K. Zhang, H. L. Hu, B. Xu, F. Q. Li and J. G. Hou, *Nanotechnology*, 2005, **16**, 1069.
2 K. H. Zheng, Y. C. Zhao, K. Deng, Z. Liu, L. F. Sun, Z. X. Zhang, L. Song, H. F. Yang, C. Z. Gu and S. S. Xie, *Appl. Phys. Lett.*, 2008, **92**, 213116.
3 D. Calestani, M. Zha, A. Zappettini, M. C. Carotta, V. Di Natale and L. Zanotti, *Sensor. Actuat. B-Chem.*, 2010, **144**, 472-478.
4 M. C. Newton, S. Firth and P. A. Warburton, *Appl. Phys. Lett.*, 2006, **89**, 072104.
5 Z. X. Zhang, L. F. Sun, Y. C. Zhao, Z. Liu, D. F. Liu, L. Cao, B. S. Zou, W. Y. Zhou, C. Z. Gu and S. S. Xie, *Nano Lett.*, 2008, **8**, 652-655.
6 W. H. Wang, J. J. Qi, Q. Y. Wang, Y. H. Huang, Q. L. Liao and Y. Zhang, *Nanoscale*, 2013, **5**, 5981-5985.
7 Y. D. Gu, J. Zhou, W. J. Mai, Y. Dai, G. Bao and Z. L. Wang, *Chem. Phys. Lett.*, 2010, **484**, 96-99.
8 K. Sun, J. J. Qi, Q. Zhang, Y. Yang and Y. Zhang, *Nanoscale*, 2011, **3**, 2166-2168.
9 R. R. Bacsa, J. Dexpert-Ghys, M. Verelst, A. Falqui, B. Machado, W. S. Bacsa, P. Chen, S. M. Zakeeruddin, M. Graetzel and P. Serp, *Adv. Func. Mater.*, 2009, **19**, 875-886.
10 F. H. Chu, C. W. Huang, C. L. Hsin, C. W. Wang, S. Y. Yu, P. H. Yeh and W. W. Wu, *Nanoscale*, 2012, **4**, 1471-1475.
11 Q. Wan, K. Yu, T. H. Wang and C. L. Lin, *Appl. Phys. Lett.*, 2003, **83**, 2253-2255.
12 K. Yu, Y. S. Zhang, R. Li. Xu, S. X. Ouyang, D. M. Li, L. Q. Luo, Z. Q. Zhu, J. Ma, S. J. Xie, S. H. Han and H. R. Geng, *Mater. Lett.*, 2005, **59**, 1866-1870.
13 A. A. Al-Tabbakh, M. A. More, D. S. Joag, I. S. Mulla and V. K. Pillai, *ACS Nano*, 2010, **4**, 5585-5590.
14 Q. H. Li, Q. Wan, Y. J. Chen, T. H. Wang, H. B. Jia and D. P. Yu, *Appl. Phys. Lett.*, 2004, **85**, 636-638.
15 W. Lei, X. B. Zhang, B. P. Wang, C. G. Lou, Z. Y. Zhu, Z. W. Zhao, C. Li and K. Hou, *IEEE Elec. Dev. Lett.*, 2008, **29**, 452-455.
16 L. M. Yu and C. C. Zhu, *Appl. Surf. Sci.*, 2009, **255**, 8359-8362.
17 Y. Chen, H. Jiang, D. Li, H. Song, Z. Li, X. Sun, G. Miao and H. Zhao, *Nanoscale Res. Lett.*, 2011, **6**, 537.
18 L. Chow, O. Lupan, H. Heinrich and G. Chai, *Appl. Phys. Lett.*, 2009, **94**, 163105.
19 D. Gedamu, I. Paulowicz, S. Kaps, O. Lupan, S. Wille, G. Haidarschin, Y. K. Mishra and R. Adelung, *Adv. Mater.*, 2014, **26**, 1541-1550.
20 Y. H. Leung, A. B. Djurisic, J. Cao, M. H. Xie and W. K. Chan, *Chem. Phys. Lett.*, 2004, **385**, 155-159.
21 G. -H. Lee, *Appl. Surf. Sci.*, 2012, **259**, 562-565.
22 H. Zhang, L. Shen and S. W. Guo, *J. Phys. Chem. C*, 2007, **111**, 12939-12943.
23 A. Roth, *Vacuum Technology*, North-Holland, Amsterdam, 2nd edn., 1982, pp. 400-405.

24 Y. B. Li, Y. Ban and D. Golberg, *Appl. Phys. Lett.*, 2004, **84**, 3603-3605.
25 Y. Sun, H. Cui, L. Gong, J. Chen, P. K. Shen and C. X. Wang, *Nanoscale*, 2011, **3**, 2978-2982.
26 X. B. Yan, B. -K. Tay and P. Miele, *Carbon*, 2008, **46**, 753-758.
27 S. S. Warule, N. S. Chaudhari, J. D. Ambekar, B. B. Kale and M. A. More, *ACS Appl. Mater. Interfaces*, 2011, **3**, 3454-3462.
28 N. S. Ramgir, I. S. Mulla, K. Vijayamohanan, D. J. Late, A. B. Bhise, M. A. More and D. S. Joag, *Appl. Phys. Lett.*, 2006, **88**, 042107.
29 X. M. Qian, H. B. Liu, Y. B. Guo, Y. L. Song and Y. L. Li, *Nanoscale Res. Lett.*, 2008, **3**, 303-307.
30 H. Jiang, J. Q. Hu, F. Gu and C. Z. Li, *Nanotechnology*, 2009, **20**, 055706.